Energy & Environmental Science

PAPER

View Article Online
View Journal | View Issue

Cite this: *Energy Environ. Sci.*, 2015, **8**, 2713

Spectroscopically tracking charge separation in polymer : fullerene blends with a three-phase morphology†

Joseph K. Gallaher,[ab] Shyamal K. K. Prasad,[ab] Mohammad A. Uddin,[c] Taehyo Kim,[d] Jin Young Kim,[d] Han Young Woo*[ce] and Justin M. Hodgkiss*[ab]

Received 2nd June 2015,
Accepted 20th July 2015

DOI: 10.1039/c5ee01713k

www.rsc.org/ees

The coexistence of intermixed amorphous polymer : fullerene phases alongside pure semicrystalline polymer and fullerene phases provides a plausible explanation for effective charge separation in organic photovoltaic blends by providing a cascaded energy landscape. We sought to test this proposal by spectroscopically tracking charge dynamics in 3-phase blends compared with binary counterparts and linking these dynamics to free charge yields. Our study applies broadband transient absorption spectroscopy to a series of closely related alternating thiophene–benzothiadiazole copolymers in which the tuned curvature of the polymer backbone controls the nature and degree of polymer–fullerene intermixing. Free charge generation is most efficient in the 3-phase morphology that features intimately mixed polymer : PCBM regions amongst neat polymer and PCBM phases. TA spectral dynamics and polarization anisotropy measurements reveal the sub-nanosecond migration of holes from intermixed to pure polymer regions of such blends. In contrast, 2-phase blends lack the spectral dynamics of this charge migration process and suffer from severe geminate recombination losses. These results provide valuable spectroscopic evidence for an efficient charge separation pathway that relies on the 3-phase morphology.

Broader context

Polymer-based solar cells promise to deliver electricity with low manufacturing costs because the active materials can be formulated as printable inks. In order to convert the tightly bound electron–hole pairs formed from photoexcitation into free charges, such devices require a bulk-heterojunction morphology. This nanostructured morphology is formed from the mixture of electron donor and acceptor components. While early studies assumed two-phase (donor and acceptor) morphologies, the coexistence of a third intermixed phase has recently been proposed as being favourable to device efficiency. In this study, we apply time-resolved absorption spectroscopy to a series of 2- *versus* 3-phase blends to compare charge generation processes in each type of blend. Our results support the idea that cascaded charge transfer from intermixed regions to phase-pure regions results in enhanced photocurrent generation.

Introduction

The phase separation morphology of polymer : fullerene organic photovoltaic (OPV) blends has long been recognized as a dominant contributor to device power conversion efficiency.[1–4] The early view was that an interpenetrating 2-phase donor/acceptor nanomorphology balanced the requirements for exciton diffusion and charge percolation.[5,6] However, the question of how charge pairs overcome their mutual Coulomb attraction to separate was not completely resolved,[7–10] in spite of the known sensitivity of charge generation photophysics to blend morphology.[11–14] More recent investigations have identified an intermixed phase in a wide range of polymer : fullerene blends.[15–24] Moreover, the cascaded energy landscape of intermixed phases interfacing with pure phases is now proposed to improve yields of charge separation and collection, possibly even resolving the vexing problem of what drives charge pair separation.[17,23–26] Intermixed polymer : fullerene phases were first identified in pBTTT : $PC_{61}BM$ blends, which exist as ordered intercalated co-crystals[15] whose

[a] *School of Chemical and Physical Sciences, Victoria University of Wellington, New Zealand. E-mail: Justin.Hodgkiss@vuw.ac.nz*
[b] *MacDiarmid Institute for Advanced Materials and Nanotechnology, New Zealand*
[c] *Department of Cogno-Mechatronics Engineering, Pusan National University, Miryang 627-706, Republic of Korea. E-mail: hywoo@pusan.ac.kr*
[d] *School of Energy and Chemical Engineering, Ulsan National Institute of Science and Technology (UNIST), Ulsan 689-798, Republic of Korea*
[e] *Department of Chemistry, Korea University, Seoul 136-713, Republic of Korea*

† Electronic supplementary information (ESI) available: Additional spectroscopic data, 2D-GIXRD, and details of spectral fitting including basis sets and residual profiles. See DOI: 10.1039/c5ee01713k

formation can be manipulated *via* structural modifications[19] and processing conditions.[27] Scarongella *et al.* recently investigated charge photogeneration channels in this system using ultrafast transient absorption (TA) spectroscopy.[28] In the 3-phase system, they resolved an electroabsorption signal that arises in the specific electrostatic environment of the co-crystal and its sub-picosecond decay reflects hole transfer into pure pBTTT crystals. Importantly, transfer of charges out of the intermixed region was found to suppress geminate charge recombination. Charge pairs are also found to be more localized and short-lived in co-crystals compared with pure phases.[29]

The intermixed phase of other blends with higher efficiency is generally amorphous rather than crystalline.[16,18,20–24] The energetic landscape found for coexisting pure and intermixed amorphous phases may provide the driving force for charge separation; fullerene crystals show >100 meV higher electron affinity than dispersed fullerene,[30] while holes may be stabilized by over 300 meV in pure polymer phases compared with amorphous intermixed phases.[31] Thus, charge pairs generated in the intermixed region may be driven into pure phases *via* this energetic bias as well as diffusion. This model is consistent with improved device efficiencies[15,17,30] and with spectroscopically resolved yields of long-lived free charges,[30] however the morphologically driven charge separation process invoked must occur on earlier timescales.

We sought to directly resolve whether charges migrate between amorphous intermixed and pure phases, and if so, establish how quickly this occurs, and how these dynamics are linked to free charge yields. We applied broadband TA spectroscopy to a series of blends where small variations in polymer backbone structure control the miscibility of fullerene, leading to controlled formation of 2- or 3-phase morphologies. By capturing the evolution of broadband (vis-NIR) TA spectra from femtosecond to microsecond timescales, we were able to identify and track spectra of holes in intermixed *versus* pure polymer phases. We found that this process happens over tens to hundreds of picoseconds in the 3-phase systems, leading to suppressed geminate charge recombination compared with the 2-phase systems where the spectral evolution attributed to interphase migration is not observed. Our findings support the idea that 3-phase morphologies provide an effective channel of charge photogeneration in OPV blends.

Results and discussion

Materials

Fig. 1 shows the molecular structures of closely related donor–acceptor low band-gap polymers; poly(5,6-bis(tetradecyloxy)-4-(thieno[3,2-*b*]thiophene-2-yl)benzo[*c*][1,2,5]thiadiazole) (PTTBT), poly(5,6-bis(tetradecyloxy)-4-(thiophen-2-yl)benzo[*c*][1,2,5]thiadiazole) (PTBT), and poly(5,6-bis(tetradecyloxy)-4-(2,2′-bithiophen-5-yl)benzo-[*c*][1,2,5]thiadiazole) (PDTBT). The different polymer backbone curvature of these polymers has been found to significantly affect fullerene miscibility and interchain stacking, and ultimately charge mobility and photovoltaic device efficiency,[32] in line

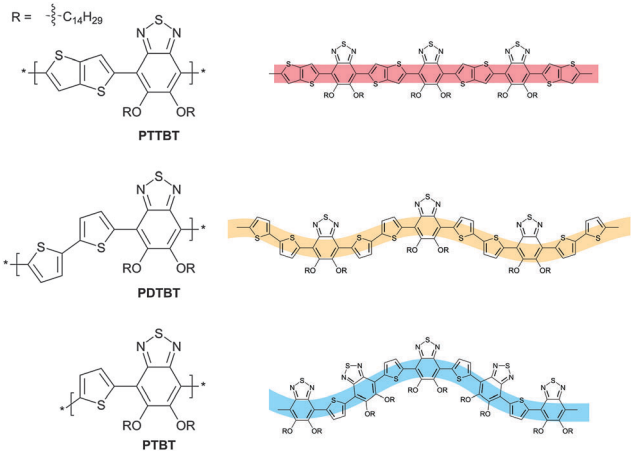

Fig. 1 Molecular structures of polymers, and schematic showing the increasing backbone curvature.

with recent work from other groups.[33,34] The synthesis and structures (including density functional theory calculations) has been reported elsewhere for PTTBT and PTBT. The backbone conformation of PDTBT (whose synthesis can be found in the Experimental section) should be similar to PTBT on account of the in-plane thiophene–BT (S···O) interactions that are common to both polymers. All polymer : fullerene blends used phenyl-C[61]-butyric acid methyl ester (PCBM) as the fullerene acceptor.

Changing the structure of the thiophene-based linkage between benzothiadiazole units, retaining the same C14 sidechains, transforms the polymer backbone from a linear shape in PTTBT to a curved shape in PTBT, while retaining a similar bandgap.[32] The new polymer PDTBT adds an intermediate member to this series through its increased spacer length. Here, the 1,4-substitution angle of thiophene rings of 160° results in decreased curvature amplitude compared to PTBT. The backbone curvature for PTBT and PDTBT is within the plane of the backbone; torsion is minimised in each of the three polymers through intrachain noncovalent S···O Coulomb interactions between partially positively charged sulphur of the linkage unit, and negatively charged oxygen on the solubilising alkoxy-sidechains.[35,36]

Morphology

Optical absorption spectroscopy and 2D grazing incidence X-ray diffraction (2D-GIXRD) measurements were used to probe how the polymers' backbone curvature influences their ordering and miscibility with PCBM. We were particularly interested in identifying the presence of 3-phase morphologies, where a strongly intermixed polymer : fullerene phase coexists with pure polymer and fullerene phases. The absorption spectra shown in Fig. 2 confirm that each of the neat polymers have a similar optical band gap of ~1.7 eV, however differences in their spectral shape are indicative of their ordering, and provide reference signatures for transient absorption studies. In particular, amorphous polymer phases have shorter conjugation lengths and differing exciton coupling compared with extended semicrystalline phases.

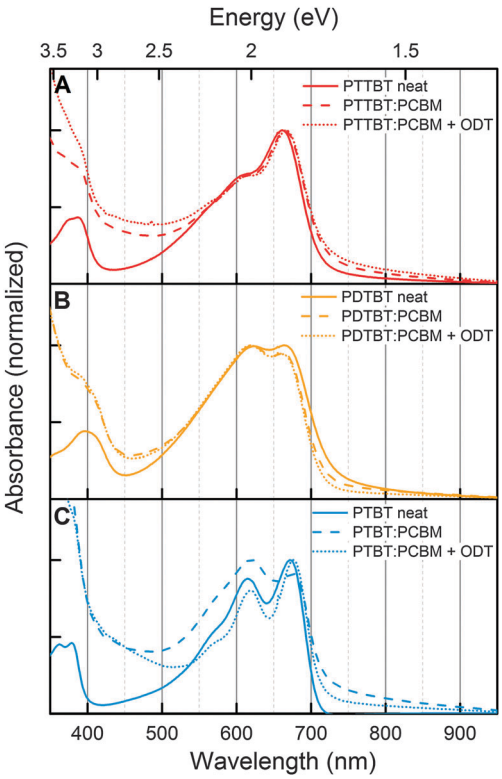

Fig. 2 Steady state optical absorption spectra of polymer and polymer : fullerene thin films cast from chlorobenzene. (A) PTTBT, (B) PDTBT, and (C) PTBT.

Fig. 2A shows that neat PTTBT has visible absorption peaks at 660 nm and 610 nm, assigned to 0–0 and 0–1 vibronic transitions, respectively. The dominant 0–0 vibronic peak is indicative of extended J-aggregate-like polymer chains that pack in ordered lamellae.[37,38] The polymer absorption spectrum is largely unchanged when blended with PCBM (1 : 1 – according to the optimum ratio in OPV devices), either with or without the octanedithiol (ODT) additive, noting that the additional absorption at $\lambda < 500$ nm is attributed to PCBM. The lack of polymer spectral perturbation from PCBM shows that highly ordered polymer stacking is retained in the blend. In agreement, a previous 2D-GIXRD investigation of this system showed that PTTBT films are highly crystalline, and the strongly ordered interchain interactions are retained in fullerene blends.[32] Additional data shown in the ESI† confirms this picture; by varying the PTTBT : PCBM blend ratio[39] from 1 : 0.2 to 1 : 4, the polymer-based scattering peaks are found not to change, while the isotropic peak due to fullerene aggregates at $q = 1.4$ Å^{-1} simply grows with increasing PCBM content. The observation of the fullerene aggregate peak with only 20% PCBM highlights the strong exclusion of PCBM of the ordered polymer aggregates. The structural and spectroscopic results demonstrate PTTBT and PCBM have poor miscibility leading to the formation of a 2-phase morphology comprising largely pure ordered polymer and PCBM phases. The possibility of an intermixed ordered (co-crystal) phase, as seen in pBTTT : PCBM blends[15,27,29,40] was ruled out in this case because the X-ray scattering peaks do not show an expanded unit cell of a PTTBT : PCBM co-crystal.

The intermediate curvature of PDTBT is reflected in the relative suppression of 0–0 vibronic peak (at 660 nm), which is comparable to the 0–1 peak at 620 nm (Fig. 2B). Weakening of the 0–0 peak results from more H- rather than J-aggregate like exciton coupling.[37,38] The lower crystallinity implied from absorption spectra of PDTBT compared with PTTBT agrees with 2D-GIXRD structural data (see ESI†). PDTBT exhibits a moderately ordered structure with out-of-plane lamellar spacing (30.6 Å) much larger than the highly crystalline PTTBT (23.0 Å). Unlike the PTTBT system above, blending PDTBT with PCBM slightly increases the interlamellae stacking distance to 33.1 Å (see ESI†), and slightly suppresses the 0–0 vibronic intensity (Fig. 2B). Processing with the ODT additive leads to recovery of the same interlamellae spacing as in neat PDTBT, but has little effect on the absorption spectrum. Importantly, the π–π stacking parameter (from 2D-GIXRD) remains the same for the PDTBT : PCBM blends (with or without the ODT additive) and for the neat polymer (4.0 Å), leading us to conclude that PCBM does not strongly infiltrate the polymer network. Thus, although not as clean as the PTTBT blend, the PDTBT : PCBM is described as having a predominantly 2-phase morphology comprised of relatively pure polymer regions, and pure PCBM clusters.

Fig. 2C shows that in the case the most curved polymer, PTBT, addition of PCBM strongly disrupts the polymer ordering. The infiltration of PCBM is indicated by the more strongly suppressed 0–0 vibronic peak. This spectroscopic observation is also consistent with the 2D-GIXRD studies shown in the ESI† and in a previous study;[32] infiltration of PCBM causes loss of the polymer π–π stacking peak, along with growth of a peak from PCBM aggregates. Both spectroscopic and scattering measurements also show that addition of the ODT cosolvent results in recovery of the polymer crystallinity due to partial demixing, evidenced by recovery of the neat polymer's vibronic progression and 2D-GIXRD scattering peaks, respectively. Thus, the PTBT : PCBM system (with an optimized 1 : 2 ratio) exhibits 3-phase behaviour; excellent miscibility results in a highly intermixed phase that can coexist with pure polymer and PCBM phases, tuned by the cosolvent. The molecular level miscibility means that even a predominantly phase separated blend is likely to be intermixed at the important interface region. This morphology has been invoked in other polymer : fullerene blends,[20,41,42] however the intermixed region was not often recognized because it is not directly detectable *via* scattering measurements, except for the case of co-crystals.[19,27] Since poor fullerene miscibility excludes the intermixed phase in PTTBT, and to a lesser extent PDTBT, this series of polymers is ideally suited to directly probing charge generation processes in the 3-phase *versus* 2-phase morphologies of closely related polymers.

Table 1 summarises the optimised polymer photovoltaic device characteristics for each polymer : PCBM blend (further details, including IPCE curves, are provided in the ESI†). The PTBT : PCBM blends are superior to the other polymers in every respect. This leads to a PCE of 5.56% when processed with ODT – more than twice the efficiency of the most efficient PTTBT blend.[32] Since these device parameters were previously shown to be uncorrelated with charge carrier mobilities (which are highest for the more crystalline linear polymer PTTBT), we undertook TA

Table 1 Summary of optimised photovoltaic device characteristics

Active layer	Additive (2%)	J_{SC} (mA cm^{-2})	V_{OC} (V)	FF	PCE (%)
PTTBT : PCBM[a] (1 : 1)	None	5.49	0.77	0.57	2.40
	ODT	7.00	0.74	0.51	2.62
PDTBT : PCBM (1 : 1)	None	4.18	0.66	0.46	1.27
	ODT	4.72	0.68	0.33	1.06
PTBT : PCBM[a] (1 : 2)	None	8.05	0.92	0.50	3.67
	ODT	9.34	0.88	0.68	5.56

[a] Reproduced from ref. 32.

spectroscopy to investigate charge photogeneration pathways in these blends.

Charge generation dynamics

While 2- and 3-phase systems are already well known, with the latter arguably a feature of all efficient blends, the present materials benefit from distinct optical signatures to compare dynamics in these systems. TA spectroscopy enabled us to establish the link between phase morphology and photocurrent generation by probing signatures of photoexcitations moving from disordered to ordered polymer regions and correlating with free charge generation. Before exploring these effects, the spectra and dynamics of excitons and charges in each of the blends were examined on early (fs–ns) timescales. The TA measurements for neat polymer and fullerene blends presented in Fig. 3 were all conducted at sufficiently low fluence to avoid annihilation and bimolecular effects, as shown in the ESI† where the dynamics are confirmed to be independent of fluence on this range.[43] TA measurements in the absence of PCBM (Fig. 3A) allowed us to first identify exciton signatures in films of each polymer and guide the interpretation of spectra (Fig. 3B) and kinetics (Fig. 3C) of blends.

For the neat PTTBT film (top), the TA spectra have a ground state bleach (GSB) feature in the visible, and a negative photo-induced absorption (labelled PIA-1) peak at ~1300 nm. The equal decay rates of all features (see ESI†) confirms the dominance of a single excitonic species with a surprisingly short lifetime of $t_{1/2}$ ~ 14 ps (Fig. 3C). The dominance of the 0–0 vibronic peak in the GSB – even more pronounced than the absorption spectrum (Fig. 3A) – shows that excitons rapidly localize onto the lowest energy extended polymer chains within the 100 fs time-resolution of the measurement.[44–47] Charge transfer is evident in the blend (top panels of Fig. 3B and C) through the emergence of a new absorption peak at ~1050 nm (labelled PIA-2), which is distinct from the broad exciton band (PIA-1). PIA-2 appears as a shoulder even at the earliest delay time (200 fs), and persists beyond the 3 ns timescale of this measurement. The new PIA-band is accompanied by a long-lived GSB signature with a dominant 0–0 peak. Consistent with numerous previous studies, this pattern of visible and near IR TA signatures indicates charge transfer to PCBM, leaving hole polarons on the polymer.[7,8,13,48,49] We also considered the possibility of polymer triplet exciton formation, which can occur on sub-ns timescales and often produces near IR PIA features similar to charges in blends of other low bandgap polymer systems.[50,51] However, the near IR TA spectrum of triplet excitons in PTTBT is quite distinct from the PCBM blend,

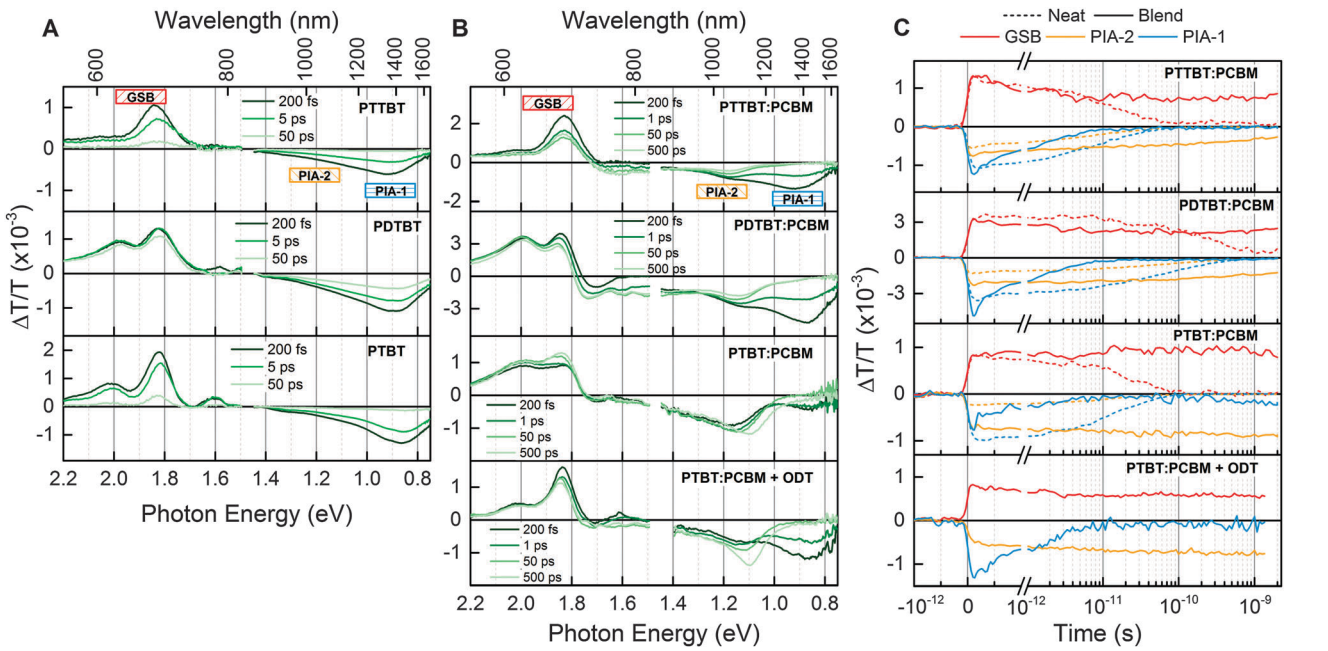

Fig. 3 Transient absorption measurements of PTTBT (top), PDTBT (middle), and PTBT (bottom) showing spectral slices at indicated time delays for neat polymer films (A), and polymer : fullerene blends (B), following 100 fs excitation at 532 nm. The spectral regions labelled GSB, PIA-1, and PIA-2 refer to the wavelength integration regions shown in the kinetic traces (C), with dashed traces corresponding to neat polymer films, and solid traces corresponding to polymer : fullerene films.

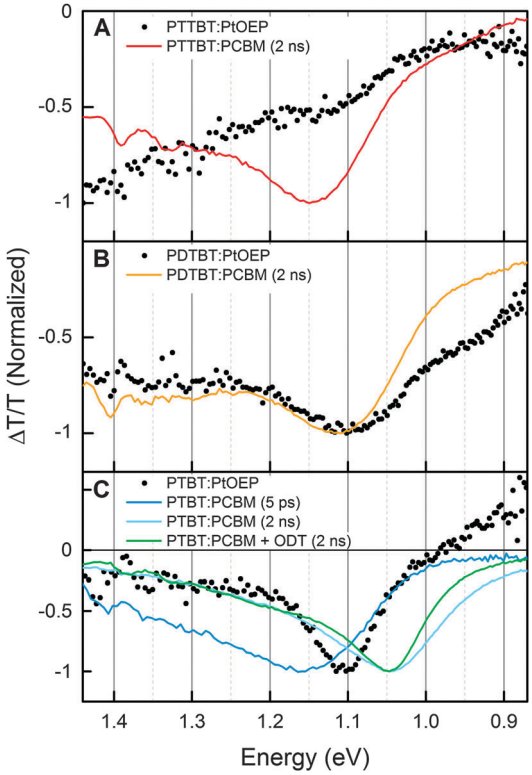

Fig. 4 Polymer triplet sensitized (polymer : PtOEP) TA spectra showing sensitized spectral shapes at 25 ns compared to the photoinduced absorption at the times indicated for (A) PTTBT : PCBM, (B) PDTBT : PCBM, and (C) PTBT : PCBM with and without ODT, at the times indicated. Excitation wavelength was 532 nm.

as demonstrated through triplet sensitization with platinum(II) 2,3,7,8,12,13,17,18-(octaethyl)porphyrin (PtOEP) in Fig. 4A. Comparing the exciton kinetics (PIA-1) of the PTTBT : PCBM blend with the neat polymer in Fig. 3C (top) confirms a reduced exciton lifetime due to charge photogeneration. However, partial GSB decay within the first 10 ps shows that some excitons decay before generating charge pairs. Since the exciton band (PIA-1) has nearly the same initial intensity in the blend as the neat polymer (relative to the GSB), it is evident that most polymer excitons are not generated in immediate proximity to PCBM acceptors, which would deplete the exciton population within our time resolution. These TA dynamics are consistent with charge photogeneration in a 2-phase morphology; the small fraction of excitons generated near polymer : fullerene interfaces generate charges on an ultrafast timescale, while other excitons are formed in polymer phases too far from fullerene acceptors to generate charges. In accordance with linear absorption spectroscopy and 2D-GIXRD studies, the cosolvent additive ODT has little effect on the TA dynamics (see ESI†). We will revisit the PTTBT : PCBM blend later when comparing charge spectral dynamics and charge recombination for the different polymers.

We now move on to the PDTBT system, whose corresponding TA spectra and kinetics are shown in the second panels of Fig. 3A–C. The analysis is broadly similar to PTTBT above, with the following differences noted: the PDTBT exciton spectrum is longer lived ($t_{1/2}$ ~ 160 ps; wavelength-independent dynamics shown in the ESI†), and with greater 0–1 vibronic intensity in the GSB compared with PTTBT. Again, the enhanced 0–0 in GSB relative to the UV-vis absorption spectrum of PDTBT shows that excitons rapidly collapse onto more extended polymer segments. The PIA bands associated with excitons (PIA-1) and charges in the PCBM blend (PIA-2) are slightly red-shifted compared with the PTTBT system, however the kinetics are similar, with excitations in the blend outliving the pristine polymer. For PDTBT, the PIA-2 peak at approximately 1100 nm is similar to the sensitized triplet exciton spectrum in Fig. 3B. However, charge photogeneration is confirmed by the growth of a sharp electroabsorption peak at ~730 nm that resembles the derivative of the ground-state absorption spectrum. This spectral signature can be seen when the electric field created by separated charge pairs perturbs the energy levels of the surrounding polymer *via* the Stark effect.[9,28] The strength of electroabsorption is sensitive to the geometric configuration of chromophores relative to the electric field, as well as the sharpness of the ground-state absorption edge. The inversion of 0–0 and 0–1 vibronic intensities in the PDTBT blend *versus* the neat polymer cannot be attributed to charges occupying more disordered polymer chains, since the 0–0 peak is likely affected by the overlapping electroabsorption. Similar to the PTTBT system above, ODT has little effect on the TA dynamics (see ESI†). The low fraction of prompt charge generation (evidenced by the high initial exciton population) and the loss of some excitons again reflects a 2-phase morphology, with domain sizes slightly exceeding the exciton diffusion length. Charge dynamics and recombination will be discussed later.

The exciton spectrum of the curved polymer PTBT (bottom panel of Fig. 3A) follows a similar pattern as the other polymers, with a wavelength-independent $t_{1/2}$ of only 18 ps, and stimulated emission evident around 775 nm in this case. However, several important differences are immediately noticeable in spectra and kinetics of the PTBT : PCBM blend (lower middle panels of Fig. 3B and C) compared with the other polymer blends. First, the low initial intensity of the exciton band (PIA-1) shows that nearly all excitons are quenched within the 200 fs time resolution of the experiment. Loss of the exciton PIA is complemented by the ultrafast appearance of a PIA band between 1000 and 1200 nm within 200 fs, which is too fast to be explained by triplet exciton formation. Together with the retention of GSB intensity, this dramatic reduction from the 18 ps exciton lifetime suggests extremely efficient charge transfer (approaching unity), as expected for a finely intermixed blend morphology that does not require excitons to diffuse to reach an interface. Secondly, the TA spectrum undergoes pronounced changes beyond the charge generation timescale; the charge-based PIA-2 band dynamically shifts to lower energy, and the relative intensity of the 0–0 band in the GSB increases. These spectral dynamics have previously been attributed to the migration of excitations from disordered polymer segments to those with larger delocalisation through chain extension (*i.e.*, ordered chains) in a closely related PTBT polymer that only differed by its shorter (C_8) sidechains.[52] In that instance, triplet formation could not

be ruled out due to overlapping spectral signatures of both species. However, for the C_{14} sidechain PTBT polymer studied here, we find that PIA-2 band in the PCBM blends is significantly broader than the sensitized triplet spectrum, and its peak shifts from higher energy than the triplet peak at early times to substantially lower energy than the relaxed triplet by 2 ns (Fig. 4C). Thus, the PIA-2 band in PTBT : PCBM is attributed to hole polarons, and the significance of the spectral dynamics will be explored below.

Unlike the previous polymer blends, the processing additive ODT induces changes to TA dynamics (Fig. 3B and C, bottom panel) that are consistent with the partial demixing of the intermixed phase, as discussed earlier from UV-visible absorption and X-ray scattering data. First, recovery of intensity in the 0–0 vibronic band of the GSB indicates formation of pure polymer domains. Second, the exciton-based PIA-1 band is now clearly resolved with a longer lifetime when ODT is used. However, ODT does not induce the strongly separated 2-phase morphology of the other polymer systems; most of the GSB intensity is retained when excitons decay, reflecting a high charge transfer yield, and significant prompt charge generation indicated by ultrafast appearance of the polaron-based PIA-2 is consistent with the higher interfacial area in the intermixed region of a 3-phase system. The polaron PIA peak undergoes a dynamic red-shift comparable to the blend lacking ODT, however in the blend with ODT, the PIA-2 peak also intensifies. Again, the spectra do not match the sensitized triplet spectrum (Fig. 4C). We considered the possibility that this growth could result from hole transfer from PCBM to PTBT, as observed in other polymer : fullerene blends.[53,54] However, hole transfer from PCBM would increase the polymer GSB intensity, in contrast to the constant GSB intensity observed during the timescale of PIA-2 dynamics. The PIA-2 peak intensities are comparable (within 15%) at 1 ns when integrating the entire bands, indicating that the apparent PIA-2 growth is due to dynamic spectral narrowing rather than population transfer.

Charge recombination dynamics

Since the sub-gap PIA-2 peak in each of the polymer : fullerene blends is attributed to hole polarons, its integrated intensity can be used to track charge dynamics. Charge recombination kinetics are examined in Fig. 5 in order to compare the long-lived extractable charge populations for each of the blends. The combination of mechanical and electronic pump–probe delay configurations allows TA dynamics to be captured from femtosecond to microsecond timescales. In all cases, excitons have fully decayed within 10 ps, so spectral overlap of exciton and polaron signatures is avoided by excluding the earliest times from the analysis. At the low excitation fluences used, recombination on early- or sub-nanosecond timescales is attributed to recombination of bound (geminate) charge pairs that would not be extractable in a device.[7,11,55] Longer lived charges exhibit strongly intensity dependent decay (see ESI†) through bimolecular recombination of free charges that would be extractable in a device.[7,11,56]

For the 2-phase PTTBT blend without ODT, approximately half of the charge population has decayed within just three

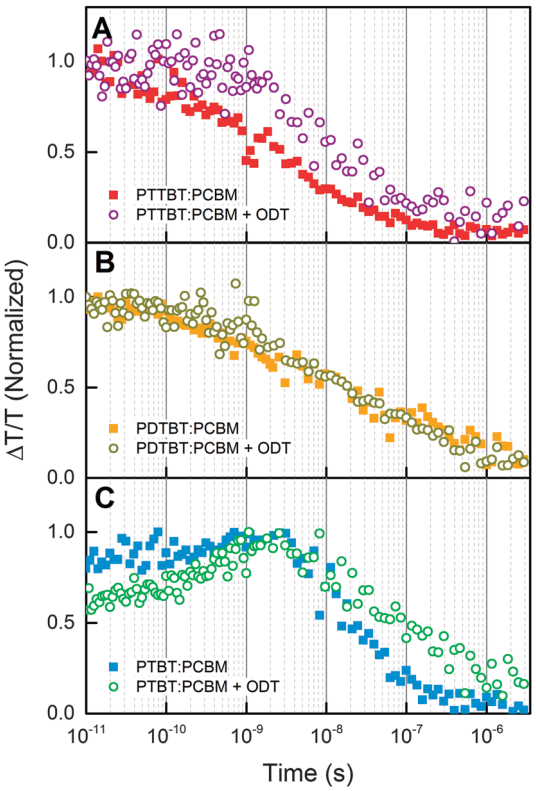

Fig. 5 Transient absorption recombination kinetics integrated over the 0.9–1.4 eV wavelength region for each polymer : PCBM processed with and without ODT additive. Each kinetic trace is normalised by the maximum intensity. All kinetic decays were collected with an excitation fluence of approximately 5 μJ cm^{-2} allowing comparison of intensity dependent decay dynamics. Spectral overlap of polarons with excitons is avoided by excluding the dynamics before 10 ps, at which time excitons have decayed.

nanoseconds – significantly faster than efficient blends previously characterised, and pointing to severe geminate recombination losses.[7] The sub-nanosecond recombination phase is suppressed when the ODT additive is used, yet a comparably small fraction (~10–20%) of charges survive beyond 100 ns. Differences in the sub-nanosecond geminate recombination dynamics show that the molecular level interfaces of PTTBT and PCBM are affected by processing with ODT. It is likely that a very low fraction of PCBM is trapped in PTTBT phases when ODT is not used; not enough PCBM to disrupt the crystallinity or form a truly intermixed phase, but enough to form a significant fraction of trapped charge pairs. Nevertheless, neither of the PTTBT blends produces appreciable yields of long-lived free charges, consistent with the poor device characteristics in Table 1.

Charge recombination dynamics for the disordered 2-phase PDTBT : PCBM blends are presented in Fig. 5B. Regardless of whether or not ODT is used, these blends also suffer significant geminate charge recombination within a few nanoseconds, and only ~30% of charges remain beyond 100 ns. Unlike the 3-phase pBTTT : PCBM system where rapid decay of electroabsorption signal reflected separation of geminate charge pairs, here the electroabsorption feature remains for the charge lifetime (see ESI†). The slightly higher long-lived charge yields compared with

the PTTBT blends is at odds with the PDTBT blends having the lowest PV device efficiencies (Table 1), which may relate to the high charge mobility for PTTBT. Nevertheless, we stress that the 2-phase PTTBT : PCBM and PDTBT : PCBM blends all have poor PV efficiencies and suffer from rapid geminate charge recombination.

Next, we examine the quality of charge separation in the PTBT : PCBM blends through the charge recombination kinetics in Fig. 5C. Whereas the PTTBT and PDTBT blends suffer substantial geminate recombination within the first 3 ns, maximal charge populations are retained at this time for the PTBT blends. The apparent PIA growth for the ODT processed blend relates to the spectral narrowing process identified in the discussion of charge generation kinetics. The suppression of rapid geminate recombination and the higher yields of long-lived charges, especially in the PTBT blend processed with ODT (>50% at 100 ns) is in line with the superior device characteristics in Table 1. The recombination kinetics for the optimized PTBT blend is also comparable to other efficient polymer : fullerene blends where well-separated charge pairs are created.[7]

Spectroscopically tracking charge migration

In order to account for the superior free charge generation observed for the PTBT : PCBM blends, we return to examine the mechanism previously invoked whereby charge pairs are separated *via* energetically biased transfer from intermixed to pure phases.[17,23,26] Just as the UV-vis absorption spectra of PTBT revealed disordered regions induced by PCBM intermixing coexisting with more phase pure regions (when processed with ODT), TA spectra can be used to probe the dynamic link between excitations occupying each of these regions. PTBT was the only polymer whose UV-visible absorption spectrum was significantly shifted upon PCBM blending and processing with ODT (Fig. 2). Likewise, the PTBT blends are the only ones to exhibit TA spectral dynamics beyond simple exciton-to-charge conversion (Fig. 3).

Fig. 6A compares the position of polaron PIA-2 peak position as a function of time for the 2-phase (PTTBT : PCBM and PDTBT : PCBM) and 3-phase (PTBT : PCBM) blends. In the 2-phase blends, the polaron PIA-2 peak remains at a constant position throughout the sub-picosecond to nanosecond timescale, and also later during recombination (shown in ESI†). Likewise, the shape of the GSB band (see ESI†) remains constant for the PTTBT blends, noting that the GSB for the PDTBT blend is obscured by the electroabsorption feature. Accordingly, the entire TA surfaces for the PTTBT : PCBM and PDTBT : PCBM, covering sub-picosecond to microsecond timescales and near IR wavelength ranges, can be accounted for using just two spectral components in a linear least-squares fit; excitons and a single polaron spectrum. The number of spectral components was guided *via* singular value decomposition, with full details of the fitting procedure given in the ESI.†

In contrast, the polaron PIA-2 peak in the 3-phase PTBT : PCBM blends (with and without ODT) dynamically red-shifts over the first hundreds of picoseconds, and then remains at a constant position during recombination (see ESI†). We showed in Fig. 4 that the PIA-2 spectral shift is unlikely to be due to

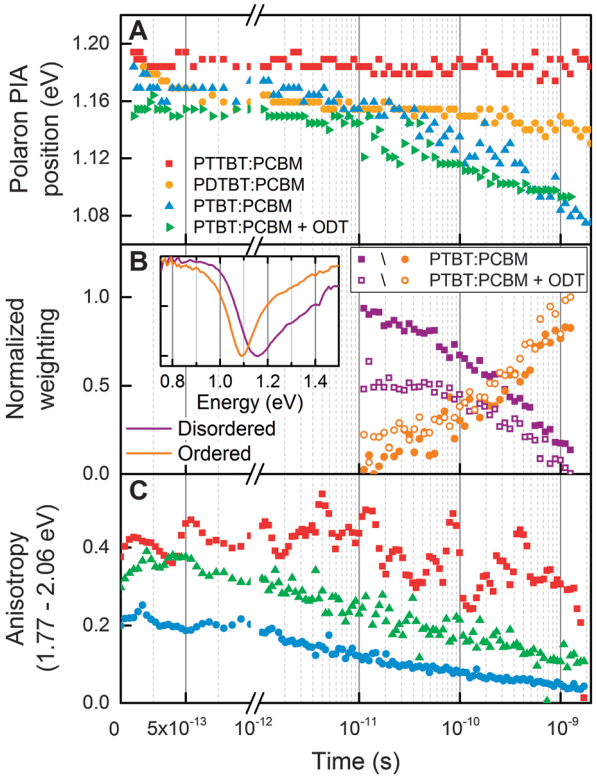

Fig. 6 Analysis of GSB and PIA dynamics in TA spectra for PTTBT : PCBM and PTBT : PCBM with and without ODT. (A) Polaron peak position as a function of time, (B) kinetics resulting from globally fitting the polaron spectral shift in PTBT : PCBM using MCR-ALS, showing the migration of charges from disordered to ordered polymer domains. (inset) The two spectral shapes used for the MCR-ALS global fit. (C) TA polarisation anisotropy showing charges are immobile in the 2-phase PTTBT : PCBM blend, and mobile in the 3-phase PTBT : PCBM.

triplet formation. For the highly mixed PTBT : PCBM blend without ODT, the PIA dynamics are also coupled with relative growth of the 0–0 vibronic peak in the GSB (see ESI†). The GSB vibronic ratio remains constant in the PTBT : PCBM blend with ODT, which, along with the lower amplitude of PIA-2 peak shift, is consistent with the lower conformational disorder revealed by UV-visible absorption and X-ray scattering. The PTBT : PCBM blends thus require an additional spectral component in a linear least squares fit of the entire TA surfaces to account for two spectrally distinct charge populations – those occupying disordered and ordered polymer chains.

The dynamics of these two charge populations in the 3-phase PTBT : PCBM blends are shown in the MCR-ALS fitting results in Fig. 6B (see ESI† for further details).[57] The figure highlights the NIR region where the two charge populations are distinguished, and excludes the first 10 ps so that an additional exciton spectrum is not required (we confirmed that the same two charge components emerge from a 3-component fit that includes the earlier exciton timescale through non-negative least squares fitting). Fig. 6B shows the time-dependent weightings of these two charge-based spectral components peaked at ~1.15 eV and ~1.05 eV, which are shown in the inset of Fig. 6B. In both PTBT : PCBM blends, the lower energy peak grows at the

expense of the higher energy peak. The nature of the spectral dynamics, and the correlation with GSB shape dynamics for the blend with the most pronounced PIA shift (the blend lacking ODT) suggests that we are observing holes migrating from disordered regions to ordered and extended polymer chains. Given that the disorder is induced by mixing with PCBM and relieved in pure polymer domains, we further attribute these spectral dynamics to the previously invoked hole migration from intermixed to phase-pure regions of the 3-phase blends.[17,23,26] This spectral assignment is supported by the observation that the amplitude of population transfer is lower for the PTBT : PCBM blend processed with ODT, where a lower fraction of charges occupy disordered polymer regions (1.15 eV PIA peak) initially (at 10 ps) due to the lower volume fraction of the intermixed region when ODT is used. We note that the data sets with- and without ODT were fit using the same pair of basis spectra, confirming that their differences relate only to the extent of population transfer.

To confirm that the spectral dynamics reflect migration of charges, we performed polarization-resolved TA spectroscopy (Fig. 6C) using a dual line visible camera to simultaneously resolve parallel and perpendicular components of the GSB signal. Anisotropy is retained near the theoretical maximum of 0.4 in the 2-phase PTTBT : PCBM blend within the 2 ns range probed. This shows that either most charges are immobile on this timescale in the 2-phase blends, or that charge motion does not depolarize the signal (which is possible in a film with highly aligned chromophores). On the other hand, the clear polarization anisotropy decay observed in the 3-phase PTBT : PCBM blends confirms that charges are mobile and lose memory of their polarization through hopping to differently oriented sites. The polarization anisotropy value for the more disordered blend is initially only $\sim$0.2, which reflects the ultrafast localization of excitations generated in orientationally disordered regions.[45,58,59] The anisotropy dynamics for the 3-phase blends occur throughout the same timescale as the spectral dynamics from hole migration in Fig. 6B, as well as on earlier timescales when exciton dynamics may also contribute.

By comparing the 3-phase PTBT : PCBM blends with the 2-phase PTTBT : PCBM and PDTBT : PCBM blends, we suggest that the higher PV efficiency of the 3 phase blends, and the higher yields of long-lived charges, is linked to the dynamics of charge migration resolved on the sub-nanosecond timescale. As illustrated in Fig. 7 and previously proposed,[17,23,25,26] the energetic disorder in 3-phase blends creates a driving force for the observed migration of holes from intermixed to pure polymer regions where they are sufficiently separated from electrons. This model may arguably be a general feature of efficient OPV blends, and it is directly confirmed in the present system because the polymer structures create a spectroscopic distinction between different charge populations. Szarko *et al.* observed a similar dynamic redshift in the PIA of holes in the PTB7 : PCBM system. They ascribed the spectral dynamics to dissociation of charge transfer states, although they considered the spectral shift be an intrinsic feature of charge separation, rather than reflecting the transfer of holes out of intermixed

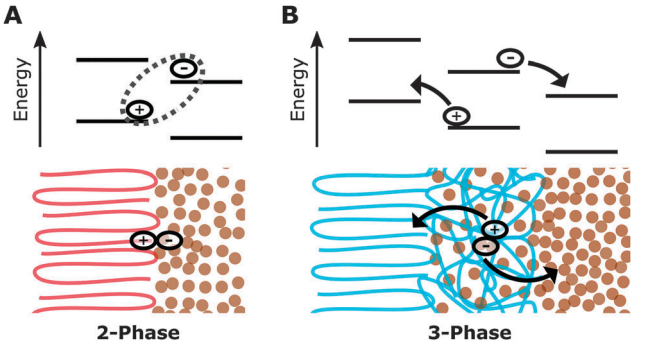

Fig. 7 Schematic of energy levels and charge behaviour in 2-phase, and 3-phase polymer : fullerene blend morphologies. (A) Charge generation in 2-phase blend yields immobile holes resulting in rapid geminate recombination and poor free charge generation. (B) The energetic disorder present in 3-phase blends yields mobile holes which are longer-lived. The energy gradient between intermixed domains and phase-pure polymer domains may be sufficient to efficiently separate charge pairs, resulting in more effective photocurrent generation.

regions.[60] Howard *et al.* also found that transient spectral shifts tracked the energetic relaxation of charges in PCDTBT : PCBM blends, which implied sufficiently enhanced early charge mobilities to account for efficient charge separation, although the phase separation morphology was not explicitly considered.[61] Although our experiment does not directly probe electron dynamics, the same argument could apply to electron migration from intermixed to pure PCBM regions.[24,29,31] The 2-phase donor/acceptor blends, on the other hand, are characterized by lack of spectral dynamics that would signify energetically biased charge migration, and concomitantly poor yields of free charges and low PV efficiencies.

Although our data suggests that the spectral shifts are unlikely to be due to triplet exciton formation, we note that even if this were the case, it would still indirectly support the proposed model of charge separation. Such triplets would be formed *via* bimolecular charge recombination[51] rather than geminate recombination because otherwise devices would perform very poorly under solar conditions. Bimolecular recombination at the densities used here would require very transiently enhanced charge mobilities in order to account for sub-nanosecond dynamics, which in turn would suggest energetically biased charge diffusion in the 3-phase morphology.

The morphologically driven separation of charges generated in intermixed regions enables the following published observations to be reconciled; relaxed charge-transfer states efficiently generate photocurrent,[10] whereas on the other hand, charges can separate at low temperature, implying that they separate during the energetic relaxation after initial charge transfer.[7] By considering the energetics of different phase regions in the present work, it is possible for charge-transfer states to dissociate into separated charges without encountering an energetic barrier, provided that pure phases are close enough to the intermixed region.

Finally, for the 3-phase PTBT : PCBM blends, the more pronounced migration of holes in the blend lacking ODT must be reconciled with its comparatively poorer performance than

the blend processed with ODT. Without ODT, the blend is dominated by the intermixed phase, as shown by the UV-vis spectrum, the initial shape of the GSB and PIA bands in the TA spectrum, and also ultrafast quenching of all excitons within just 200 fs. In such a morphology, the minor volume fractions of phase-pure polymer and fullerene are unlikely to be well connected in percolating pathways. Thus, while charge pairs may be initially well separated *via* energetically driven transport to a nearby phase pure region, they may become trapped there, suppressing the current and fill-factor of the device. The requirement for phase pure percolation pathways was also highlighted for other 3-phase blends.[23,28] The ODT processed PTBT : PCBM film presents a better balance of intermixed regions to phase pure regions, shown by the greater fraction of ordered polymer spectral signatures and the lower fraction of prompt (ultrafast) charge generation. This well-balanced 3-phase morphology results in effective charge separation as well as percolating pathways for extracting charges from the device. Moreover, the presence of intermixed layers between phase pure regions can act as an energetic barrier to prevent interfacial charge recombination when charges are more stable in the phase pure regions. In the future, varying the polymer molecular weight may prove to be an effective means of finely tuning the balance of intermixed and phase pure regions.

It may also be argued that the intermixed regions may act as a barrier towards excitons reaching charge separating interfaces from polymer phases, which might suppress charge photogeneration for 3-phase systems. However, two known mechanisms can alleviate this problem; firstly, excitons are very delocalized on the sub-picosecond timescale of charge generation, effectively allowing long-range electron transfer.[47] Secondly, 2-step processes whereby energy transfer to fullerenes precedes hole transfer to the polymer has been shown in both molecular dyads,[62] and strongly intermixed films.[63] Formation of an intermediate fullerene excitation would result in decay, then recovery, of the polymer-based GSB signal, however these spectral dynamics would not be apparent if hole transfer was fast.

Conclusions

We investigated charge photogeneration pathways in fullerene blends of a series of three closely related copolymers where differences in the backbone connectivity induces varying degrees of curvature. These structural differences are manifest in their phase behaviour in PCBM blends; the linear and weakly curved polymers PTTBT and PDTBT form 2-phase morphologies with PCBM, whereas PCBM is more miscible with the curved polymer PTBT, which leads to the coexistence of intermixed and phase pure regions that can be balanced through cosolvent processing. Since these phases present spectroscopic signatures, we were able to track the motion of hole polarons between disordered and ordered regions and link these dynamics to yields of long-lived charges and overall PV efficiencies. For the polymers whose rigid backbones lead to 2-phase blends lacking an intermixed region, the lack of spectral dynamics and the polarization anisotropy retention shows that holes are immobile. Rapid geminate charge recombination and poor photovoltaic performance are observed in such blends. In contrast, the 3-phase morphology supported by the polymer with a curved backbone exhibits highly mobile holes that are observed to migrate from the intermixed domains to phase-pure polymer domains. Such blends feature longer-lived populations of extractable charges and concomitantly better device performance. The energy gradient between the intermixed and phase-pure regions may be sufficient to efficiently separate charge pairs and prevent subsequent recombination, with free charges subsequently percolating through the phase-pure domains. These results provide valuable spectroscopic evidence for this pathway of efficient charge separation and its link to blend morphology and polymer structure.

Experimental section

Materials

The detailed synthetic procedures for PTTBT and PTBT were reported in a previous paper.[32]

Poly(5,6-bis(tetradecyloxy)-4-(2,2′-bithiophen-5-yl)benzo[*c*]-[1,2,5]thiadiazole) (PDTBT). In a glove box, 5,5-bis(trimethylstannyl)-2,2-bithiophene (180 mg, 0.366 mmol), 4,7-dibromo-5,6-bis(tetradecyloxy)benzo[*c*][1,2,5]thiadiazole (263 mg, 0.366 mmol), tris(dibenzylideneacetone)dipalladium(0) (3 mol%) and tri(*o*-tolyl)-phosphine (8 mol%) were added in a 5 mL microwave vial. The vial was sealed and chlorobenzene (3.5 mL) was added. The polymerization reaction was carried out in a microwave reactor: 10 min at 80 °C, 10 min at 100 °C, 40 min at 140 °C. The polymer was end-capped by addition of 0.1 equiv. of 2-(tributylstannyl)thiophene and reacted further at 140 °C for 20 min. The polymer solution was cooled down and 0.2 equiv. of 2-bromothiophene was added by syringe and the reaction solution was further reacted at 140 °C for 20 min. The crude polymer was precipitated into a mixture of methanol : HCl (350 mL : 10 mL) and purified by Soxhlet extraction with acetone, hexane and chloroform. The dissolved portion in chloroform was concentrated under reduced pressure and precipitated into cold methanol. The polymer was dried under vacuum for 24 h. Yield: 86%. ^{1}H NMR (300 MHz, $CDCl_3$): δ (ppm) 8.54 (br, 2H), 7.39 (br, 2H), 4.18 (br, 4H), 2.00 (br, 8H), 1.65–1.20 (m, 36H), 1.14–0.85 (m, 10H). Number-average molecular weight (GPC, *o*-dichlorobenzene): M_n = 10 000 g mol^{-1} (PDI = 2.1).

Photovoltaic device fabrication

The photovoltaic device was fabricated with a configuration of glass/indium-tin-oxide (ITO)/PEDOT : PSS/active layer/Al. For bulk-heterojunction (BHJ) devices, the mixtures of polymer and PCBM in chlorobenzene (1–2 wt%) were spin coated with and without a processing additive (ODT, 2 vol%) on top of the PEDOT : PSS layer at 700–1500 rpm for 60 s inside a glove box. The optimized polymer : PCBM blend ratio was determined to be 1 : 1, 1 : 1, and 1 : 2 for PTTBT, PDTBT and PTBT, respectively. Subsequently, the device was pumped down under vacuum ($<10^{-6}$ Torr), and Al (100 nm) was deposited. The area of the

Al electrode defines an active area of the device as 13.0 mm^2. Measurements were carried out inside a glove box from a solar simulator (AM 1.5G illumination at 100 mW cm^{-2}) equipped with a Keithley 2635A source measurement unit. The incident photon-to-current efficiency (IPCE) measurements were performed using a PV measurement QE system using a monochromatic light from a xenon lamp under ambient conditions. The monochromatic light was chopped at 100 Hz and intensity was calibrated relative to a standard Si photodiode using a lock-in-amplifier.

2D-GIXRD measurements

The 2D-GIXRD measurements were carried out on a PLS-II 3A SAXS beam line at Pohang Accelerator Laboratory, S. Korea. The detailed measurement conditions were reported previously.[31] The samples for 2D-GIXRD measurements were prepared by spin coating of the polymer or polymer : PCBM blend with/without ODT under the same condition for photovoltaic device fabrication.

Optical spectroscopy sample preparation

Steady state UV-vis absorption spectra were collected using an Agilent 8453 UV-visible spectrophotometer over the range 220–1100 nm. All photophysical measurements were conducted on thin film samples cast on Spectrosil quartz substrates. All films were spun cast from chlorobenzene at 1500 rpm for 60 seconds, with the concentration of stock solutions given below. The polymer : fullerene blend ratios for spectroscopic measurements were chosen based on the optimised device results. For polymer : PCBM blends processed with additive, ODT (2 vol%) was added to each stock solution of PCBM before combining with polymer stock solutions, and then mixed for 2 hours before casting (Table 2).

For triplet sensitized measurements, thin film samples were prepared from a stock solution of polymer (matching the concentration used for each neat sample) doped with 40 wt% PtOEP (with respect to the polymer) in chlorobenzene. Steady state UV-vis absorption for these films are shown below.

Transient absorption spectroscopy

All samples were measured under dynamic vacuum (10^{-5} mbar) using a homebuilt sample chamber. TA spectroscopy was carried out using an amplified Ti–sapphire laser (Spectra Physics, 100 fs pulse duration, 800 nm, 3 kHz). The broadband probe pulses were generated *via* two different methods. Visible wavelengths (550–850 nm) were generated using a homebuilt non-collinear optical parametric amplifier (NOPA) based on ref. 64, pumped by a fraction of output from the amplifier. Infrared wavelengths (830–1700 nm) were generated by focusing a small portion of output from the amplifier in a 3 mm YAG window.

After transmission through the sample, visible probe pulses were coupled into a spectrograph (Acton SP2150, Princeton Instruments, 150 lines per millimetre grating) using optical fibres, and referenced to a probe pulse that was not transmitted through the sample. IR probe pulses were transmitted through an 830 nm long pass filter before reaching the sample chamber and then spectrally dispersed using a homebuilt prism based polychromator after transmission through the sample. Probe shots were read out at 3 kHz using a camera controller (Stresing) equipped with a dual channel linear Si photodiode array (visible) and a single channel linear InGaAs photodiode array (IR). The differential transmission signal ($\Delta T/T$) is calculated using sequential probe shots corresponding to pump on *vs.* off, where the excitation repetition rate is $\omega/2$. In a typical measurement, 2000 shots were averaged per time point and a time series were repeated 5 times.

For ultrafast (<3 ns) measurements, an optical parametric amplifier (TOPAS) provided 100 fs excitation pulses at 532 nm, which were chopped at 1.5 kHz. The excitation beam was attenuated to achieve an excitation intensity of approximately 5 μJ cm^{-2}. The observation of comparable dynamics at higher fluence confirmed bimolecular effects were insignificant on sub-nanosecond timescales. The relative delay between pump and probe pulses was varied using an automated delay stage (Newport). For charge recombination measurements (ns–ms), excitation pulses were obtained using the 2nd harmonic (532 nm) of a Q-switched Nd:YVO_4 laser (AOT-YVO-25QSP, 700 ps) which was synchronized with the amplifier output. Excitation intensities were varied (0.4–41.6 μJ cm^{-2}) and each measurement were averaged 1000 shots per time point, with the number of repeat scans to achieve sufficient signal:noise and account for signal strength at different intensities. The delay between pump and probe pulses was varied using an electronic delay generator (Stanford Research Systems DG535).

All transient absorption data was processed using MATLAB, starting with chirp correction for ultrafast measurements and combining visible and IR components. In the cases where excitation densities were not identical for visible and IR measurements of the same sample, IR spectra were re-scaled by the ratio of excitation fluences used. Observing a smooth transition between data in the visible and IR wavelength ranges after correction verified the validity of this procedure.

Table 2 Thin film casting solutions

Sample	Total component concentrations (mg mL^{-1})
Neat PTTBT	7.5
PTTBT : PCBM (1 : 1)	22.2
Neat PDTBT	16.7
PDTBT : PCBM (1 : 1)	22.2
Neat PTBT	11.1
PTBT : PCBM (1 : 2)	22.2

Acknowledgements

JKG, SKKP, and JMH acknowledge the support of a Rutherford Discovery Fellowship. This work was supported by the National Research Foundation (NRF) of Korea (2012M3A6A7055540, 2013M3C1A3065522).

Notes and references

1 A. J. Moulé and K. Meerholz, *Adv. Funct. Mater.*, 2009, **19**, 3028–3036.

2 F. Liu, Y. Gu, J. W. Jung, W. H. Jo and T. P. Russell, *J. Polym. Sci., Part B: Polym. Phys.*, 2012, **50**, 1018–1044.
3 A. Pivrikas, H. Neugebauer and N. S. Sariciftci, *Sol. Energy*, 2011, **85**, 1226–1237.
4 B. C. Thompson and J. M. J. Fréchet, *Angew. Chem., Int. Ed.*, 2008, **47**, 58–77.
5 S. Günes, H. Neugebauer and N. S. Sariciftci, *Chem. Rev.*, 2007, **107**, 1324–1338.
6 K. M. Coakley and M. D. McGehee, *Chem. Mater.*, 2004, **16**, 4533–4542.
7 A. J. Barker, K. Chen and J. M. Hodgkiss, *J. Am. Chem. Soc.*, 2014, **136**, 12018–12026.
8 A. A. Bakulin, A. Rao, V. G. Pavelyev, P. H. M. van Loosdrecht, M. S. Pshenichnikov, D. Niedzialek, J. Cornil, D. Beljonne and R. H. Friend, *Science*, 2012, **335**, 1340–1344.
9 S. Gelinas, A. Rao, A. Kumar, S. L. Smith, A. W. Chin, J. Clark, T. S. van der Poll, G. C. Bazan and R. H. Friend, *Science*, 2013, **343**, 512–516.
10 K. Vandewal, S. Albrecht, E. T. Hoke, K. R. Graham, J. Widmer, J. D. Douglas, M. Schubert, W. R. Mateker, J. T. Bloking, G. F. Burkhard, A. Sellinger, J. M. J. Fréchet, A. Amassian, M. K. Riede, M. D. McGehee, D. Neher and A. Salleo, *Nat. Mater.*, 2014, **13**, 63–68.
11 I. A. Howard, R. Mauer, M. Meister and F. Laquai, *J. Am. Chem. Soc.*, 2010, **132**, 14866–14876.
12 R. Alex Marsh, J. M. Hodgkiss, S. Albert-Seifried and R. H. Friend, *Nano Lett.*, 2010, **10**, 923–930.
13 J. Guo, H. Ohkita, S. Yokoya, H. Benten and S. Ito, *J. Am. Chem. Soc.*, 2010, **132**, 9631.
14 J. Piris, T. E. Dykstra, A. A. Bakulin, P. H. M. Van Loosdrecht, W. Knulst, M. T. Trinh, J. M. Schins and L. D. A. Siebbeles, *J. Phys. Chem. C*, 2009, **113**, 14500–14506.
15 A. C. Mayer, M. F. Toney, S. R. Scully, J. Rivnay, C. J. Brabec, M. Scharber, M. Koppe, M. Heeney, I. McCulloch and M. D. McGehee, *Adv. Funct. Mater.*, 2009, **19**, 1173–1179.
16 W. Yin and M. Dadmun, *ACS Nano*, 2011, **5**, 4756–4768.
17 W. Chen, T. Xu, F. He, W. Wang, C. Wang, J. Strzalka, Y. Liu, J. Wen, D. J. Miller, J. Chen, K. Hong, L. Yu and S. B. Darling, *Nano Lett.*, 2011, **11**, 3707–3713.
18 B. A. Collins, J. R. Tumbleston and H. Ade, *J. Phys. Chem. Lett.*, 2011, **2**, 3135–3145.
19 N. C. Miller, E. Cho, R. Gysel, C. Risko, V. Coropceanu, C. E. Miller, S. Sweetnam, A. Sellinger, M. Heeney, I. McCulloch, J. L. Brédas, M. F. Toney and M. D. McGehee, *Adv. Energy Mater.*, 2012, **2**, 1208–1217.
20 M. A. Ruderer, R. Meier, L. Porcar, R. Cubitt and P. Müller-Buschbaum, *J. Phys. Chem. Lett.*, 2012, **3**, 683–688.
21 H. W. Ro, B. Akgun, B. T. O'Connor, M. Hammond, R. J. Kline, C. R. Snyder, S. K. Satija, A. L. Ayzner, M. F. Toney, C. L. Soles and D. M. DeLongchamp, *Macromolecules*, 2012, **45**, 6587–6599.
22 P. Kohn, Z. Rong, K. H. Scherer, A. Sepe, M. Sommer, P. Müller-Buschbaum, R. H. Friend, U. Steiner and S. Hüttner, *Macromolecules*, 2013, **46**, 4002–4013.
23 P. Westacott, J. R. Tumbleston, S. Shoaee, S. Fearn, J. H. Bannock, J. B. Gilchrist, S. Heutz, J. DeMello, M. Heeney, H. Ade, J. R. Durrant, D. S. McPhail and N. Stingelin, *Energy Environ. Sci.*, 2013, **6**, 2756.
24 B. A. Collins, Z. Li, J. R. Tumbleston, E. Gann, C. R. Mcneill and H. Ade, *Adv. Energy Mater.*, 2013, **3**, 65–74.
25 C. Groves, *Energy Environ. Sci.*, 2013, **6**, 1546–1551.
26 T. M. Burke and M. D. McGehee, *Adv. Mater.*, 2014, **26**, 1923–1928.
27 E. Buchaca-Domingo, A. J. Ferguson, F. C. Jamieson, T. McCarthy-Ward, S. Shoaee, J. R. Tumbleston, O. G. Reid, L. Yu, M.-B. Madec, M. Pfannmöller, F. Hermerschmidt, R. R. Schröder, S. E. Watkins, N. Kopidakis, G. Portale, A. Amassian, M. Heeney, H. Ade, G. Rumbles, J. R. Durrant and N. Stingelin, *Mater. Horiz.*, 2014, **1**, 270.
28 M. Scarongella, J. De Jonghe-Risse, E. Buchaca-Domingo, M. Causá, Z. Fei, M. Heeney, J.-E. Moser, N. Stingelin and N. Banerji, *J. Am. Chem. Soc.*, 2015, **137**, 2908–2918.
29 F. Dou, E. Buchaca-Domingo, M. Sakowicz, E. Rezasoltani, T. McCarthy-Ward, M. Heeney, X. Zhang, N. Stingelin and C. Silva, *J. Mater. Chem. C*, 2015, **3**, 3722–3729.
30 F. C. Jamieson, E. B. Domingo, T. McCarthy-Ward, M. Heeney, N. Stingelin and J. R. Durrant, *Chem. Sci.*, 2012, **3**, 485.
31 S. Sweetnam, K. R. Graham, G. O. Ngongang Ndjawa, T. Heumüller, J. A. Bartelt, T. M. Burke, W. Li, W. You, A. Amassian and M. D. McGehee, *J. Am. Chem. Soc.*, 2014, **136**, 14078–14088.
32 W. Lee, G.-H. Kim, S. Ko, S. Yum, S. Hwang, S. Cho, Y. Shin, J. Y. Kim and H. Y. Woo, *Macromolecules*, 2014, **47**, 1604–1612.
33 Y. Wu, Z. Li, W. Ma, Y. Huang, L. Huo, X. Guo, M. Zhang, H. Ade and J. Hou, *Adv. Mater.*, 2013, **25**, 3449–3455.
34 G. Zuo, Z. Li, M. Zhang, X. Guo, Y. Wu, S. Zhang, B. Peng, W. Wei and J. Hou, *Polym. Chem.*, 2014, **5**, 1976.
35 W. Lee, H. Choi, S. Hwang, J. Y. Kim and H. Y. Woo, *Chem. – Eur. J.*, 2012, **18**, 2551–2558.
36 S. V Meille, A. Farina, F. Bezziccheri and M. C. Gallazzi, *Adv. Mater.*, 1994, **6**, 848–851.
37 F. C. Spano and C. Silva, *Annu. Rev. Phys. Chem.*, 2014, **65**, 477–500.
38 J. Clark, C. Silva, R. Friend and F. Spano, *Phys. Rev. Lett.*, 2007, **98**, 206406.
39 J. A. Bartelt, Z. M. Beiley, E. T. Hoke, W. R. Mateker, J. D. Douglas, B. A. Collins, J. R. Tumbleston, K. R. Graham, A. Amassian, H. Ade, J. M. J. Fréchet, M. F. Toney and M. D. Mcgehee, *Adv. Energy Mater.*, 2013, **3**, 364–374.
40 M. Scarongella, A. A. Paraecattil, E. Buchaca-Domingo, J. D. Douglas, S. Beaupré, T. McCarthy-Ward, M. Heeney, J.-E. Moser, M. Leclerc, J. M. J. Fréchet, N. Stingelin and N. Banerji, *J. Mater. Chem. A*, 2014, **2**, 6218.
41 B. A. Collins, E. Gann, L. Guignard, X. He, C. R. McNeill and H. Ade, *J. Phys. Chem. Lett.*, 2010, **1**, 3160–3166.
42 B. Watts, W. J. Belcher, L. Thomsen, H. Ade and P. C. Dastoor, *Macromolecules*, 2009, **42**, 8392–8397.
43 J. M. Hodgkiss, S. Albert-Seifried, A. Rao, A. J. Barker, A. R. Campbell, R. A. Marsh and R. H. Friend, *Adv. Funct. Mater.*, 2012, **22**, 1567–1577.
44 E. Collini and G. D. Scholes, *Science*, 2009, **323**, 369–373.

45 T. E. Dykstra, E. Hennebicq, D. Beljonne, J. Gierschner, G. Claudio, E. R. Bittner, J. Knoester and G. D. Scholes, *J. Phys. Chem. B*, 2009, **113**, 656–667.
46 N. Banerji, *J. Mater. Chem. C*, 2013, **1**, 3052.
47 K. Chen, A. J. Barker, M. E. Reish, K. C. Gordon and J. M. Hodgkiss, *J. Am. Chem. Soc.*, 2013, **135**, 18502–18512.
48 J. Guo, H. Ohkita, H. Benten and S. Ito, *J. Am. Chem. Soc.*, 2009, **131**, 16869–16880.
49 H. Ohkita, S. Cook, Y. Astuti, W. Duffy, S. Tierney, W. Zhang, M. Heeney, I. McCulloch, J. Nelson, D. D. C. Bradley and J. R. Durrant, *J. Am. Chem. Soc.*, 2008, **130**, 3030–3042.
50 A. Rao, P. C. Y. Chow, S. Gélinas, C. W. Schlenker, C. Li, H. Yip, A. K.-Y. Jen, D. S. Ginger and R. H. Friend, *Nature*, 2013, **500**, 435–439.
51 F. Etzold, I. Howard, N. Forler, A. Melnyk, D. Andrienko, M. R. Hansen and F. Laquai, *Energy Environ. Sci.*, 2015, **8**, 1511.
52 M. E. Reish, G. S. Huff, W. Lee, M. A. Uddin, A. J. Barker, J. K. Gallaher, J. M. Hodgkiss, H. Y. Woo and K. C. Gordon, *Chem. Mater.*, 2015, **28**, 2770–2779.
53 A. A. Bakulin, S. D. Dimitrov, A. Rao, P. C. Y. Chow, C. B. Nielsen, B. C. Schroeder, I. McCulloch, H. J. Bakker, J. R. Durrant and R. H. Friend, *J. Phys. Chem. Lett.*, 2013, **4**, 209–215.
54 A. A. Bakulin, J. C. Hummelen, M. S. Pshenichnikov and P. H. M. Van Loosdrecht, *Adv. Funct. Mater.*, 2010, **20**, 1653–1660.
55 J. M. Hodgkiss, A. R. Campbell, R. A. Marsh, A. Rao, S. Albert-Seifried and R. H. Friend, *Phys. Rev. Lett.*, 2010, **104**, 1–4.
56 C. G. Shuttle, R. Hamilton, B. C. O'Regan, J. Nelson and J. R. Durrant, *PNAS*, 2010, **107**, 16448–16452.
57 J. Jaumot, A. de Juan and R. Tauler, *Chemom. Intell. Lab. Syst.*, 2015, **140**, 1–12.
58 P. Parkinson, C. Müller, N. Stingelin, M. B. Johnston and L. M. Herz, *J. Phys. Chem. Lett.*, 2010, **1**, 2788–2792.
59 M. Chang, M. Frampton, H. Anderson and L. Herz, *Phys. Rev. Lett.*, 2007, **98**, 027402.
60 J. M. Szarko, B. S. Rolczynski, S. J. Lou, T. Xu, J. Strzalka, T. J. Marks, L. Yu and L. X. Chen, *Adv. Funct. Mater.*, 2014, **24**, 10–26.
61 I. A. Howard, F. Etzold, F. Laquai and M. Kemerink, *Adv. Energy Mater.*, 2014, **4**, 1–9.
62 P. van Hal, R. Janssen, G. Lanzani, G. Cerullo, M. Zavelani-Rossi and S. De Silvestri, *Phys. Rev. B: Condens. Matter Mater. Phys.*, 2001, **64**, 1–7.
63 A. R. S. Kandada, G. Grancini, A. Petrozza, S. Perissinotto, D. Fazzi, S. S. K. Raavi and G. Lanzani, *Sci. Rep.*, 2013, **3**, 2073.
64 C. Manzoni, D. Polli and G. Cerullo, *Rev. Sci. Instrum.*, 2006, **77**, 023103.

